2

DIRECT EVIDENCE OF PLASMA-DENSITY
STRUCTURING IN THE AURORAL
F-REGION IONOSPHERE

R.T. Tsunoda, I. Häggström,
A. Pellinen-Wannberg, Å. Steen,
and G. Wannberg

DIRECT EVIDENCE OF PLASMA-DENSITY STRUCTURING
IN THE AURORAL F-REGION IONOSPHERE

by

R.T. Tsunoda*, I. Häggström, A. Pellinen-Wannberg,
A. Steen, and G. Wannberg
Kiruna Geophysical Institute
P.O. Box 704, S-981 27 Kiruna, Sweden

*) On leave from SRI International, Menlo Park, CA 94025 U.S.A

ABSTRACT

We investigate the hypothesis that large-scale (~100 km) plasma-density enhancements (or "blobs") found in the auroral F layer become structured via a magnetic-flux-tube interchange (MFTI) process. In such a process, plasma structure is produced when spatially irregular electric fields transport higher number-density plasma (from within the blob) into a region containing lower number-density plasma (the background ionosphere), and vice versa. Direct experimental evidence of this process can be obtained by measuring concurrently the spatial distributions of F-region plasma density and electric field. Using the tristatic EISCAT radar facility, we measured these quantities in a two-dimensional plane transverse to the geomagnetic field, at 300-km altitude. We show, in a case study, that plasma-density structure found along the poleward wall of a blob was indeed accompanied by similar-scale variations in the ionospheric electric field, and that the sense of relative motion between high- and low-number-density plasma is consistent with ongoing structuring of the plasma via an MFTI process. From the estimated growth rate of 3×10^{-3} s^{-1}, the observed plasma structure would have been produced in several minutes by the irregular electric field pattern. The source of the MFTI process, however, is not clear. The MFTI process did not appear to be driven by F-region polarization electric fields, a conclusion based on (1) the apparent lack of inverse correlation between plasma density and "slip" velocity (i.e., difference velocity between plasma and neutrals) patterns, and (2) the positive growth rate found along the poleward wall of the blob in the presence of a westward Pedersen current. This conclusion excludes (at least for this data set) the gradient-drift and current-convective instabilities as primary sources of the ongoing structuring process.

2

I. INTRODUCTION

The existence of large-scale plasma-density enhancements, or "blobs," in the auroral F layer has now been reported by a number of researchers [e.g., Banks et al., 1974; Vickrey et al., 1980; Kelley et al., 1982; Robinson et al., 1982, 1984; Tsunoda and Vickrey, 1984; Tsunoda et al., 1984; Weber et al., 1984]. Although the source mechanism for blob production is not yet known with any certainty, the above-mentioned researchers have suggested soft-particle precipitation and solar-produced ionization as possible candidates. Blob dimensions are typically 100 km in latitude, few hundred km in altitude (along geomagnetic field lines), and several-to-many 100 km in longitude. Peak plasma densities in these enhancements range from 10^5 el/cm^3 during solar activity minimum to more than 10^6 el/cm^3 during solar activity maximum.

One of the more intriguing features of the auroral F layer is that kilometer-scale (i.e., scintillation producing) plasma-density irregularities appear to be confined to the vicinity of blobs. This observation naturally points to the plasma-density gradient associated with a wall of a blob and an ionospheric electric field as sources of free energy for further irregularity production at scale sizes smaller than the blob itself. In other words, it is tempting to envision an irregularity cascade process [e.g., Kelley et al., 1982] in which smaller scale irregularities are produced by the fragmentation of larger scale irregularities, of which the blob represents the largest scale size. For example, Vickrey et al. [1980] found that locally-intense, radio-wave scintillations were associated with blobs. They suggested that localized km-scale irregularities (in plasma density) responsible for scintillations were produced by the current-convective [Ossakow and Chaturvedi, 1979] and gradient-drift [Simon, 1963; Linson and Workman, 1970; Keskinen and Ossakow, 1982] instabilities acting on the walls of blobs.

If such an irregularity cascade process (e.g., driven by the gradient-drift instability) is operative along the wall of a blob, it

3

would be desirable to characterize that structure in a way that the source mechanism could be identified. The gradient-drift instability is an MFTI process which produces a structured pattern in plasma density that is most apparent when viewed in a two-dimensional plane transverse to the geomagnetic field (at F-region altitudes). In fact, computer simulations of this instability process are most often illustrated in this plane [e.g., Keskinen and Ossakow, 1982]. The only known technique for obtaining the plasma density distribution in more than one dimension is the incoherent scatter radar. Even with this technique, it is extremely difficult to separate spatial variations from temporal variations, especially if we attempt to map too large a volume of space with the radar.

Tsunoda and Vickrey [1984] used a different approach to this problem of minimizing ambiguity between spatial and temporal variations. By operating the Chatanika incoherent-scatter radar in a rapid meridian-scan mode, and allowing a blob to zonally convect through the scanned sector, they were able to reconstruct two-dimensional cross-sections of a blob at several altitudes in planes transverse to the geomagnetic field. This "bread-slice" technique of mapping the three-dimensional configuration of a blob is thought to be a viable approach because plasma in the F layer is virtually incompressible and its spatial distribution is dominated by convection, not production and loss. This is certainly the case for time scales (2 to 5 minutes) associated with the bread-slice technique. Tsunoda and Vickrey [1984] showed in a case study that a blob was indeed structured as a function of longitude along one wall, and that the measured neutral wind directed out of that wall was consistent with the required driver for the gradient-drift instability.

Despite the circumstantial evidence presented thus far [Vickrey et al., 1980; Tsunoda and Vickrey, 1984] in support of the gradient-drift and current-convective instabilities operating in the auroral F-region ionosphere, there remain serious questions as to their effective growth rate for irregularity production because of the frequent presence of a highly-conducting, auroral E layer beneath blobs. It is well known that

4

polarization electric fields set up by these instabilities can be short-circuited by closure currents through a conducting E layer [e.g., Haerendel et al., 1967, 1969; Volk and Haerendel, 1971; Shiau and Simon, 1974; Vickrey and Kelley, 1982]. For example, Vickrey et al. [1980] estimated the ratio of height-integrated Pedersen conductivity (or Pedersen conductance) in the E layer to that in the F layer to be (in their case) about 100. Because the auroral E layer is almost always present beneath F-region blobs, the possibility of polarization shorting cannot be ignored.

The irregularity growth rates of these instabilities can be further reduced (even in the case of partial current closure) by velocity-shear effects produced by an electric field component parallel to the plasma density gradient [e.g., Perkins and Doles, 1975; Zalesak et al., 1982]. North-south electric fields that are parallel to plasma-density gradients of east-west-aligned blobs commonly occur in the auroral ionosphere. In fact, north-south electric fields dominate over east-west electric fields in the evening and morning sectors where convective flow is almost purely zonal.

Given that the F-region polarization electric field is susceptible to significant reduction by E-region shorting (and velocity shear effects), we should (1) not accept proposed mechanisms for irregularity production in the auroral F region (such as the gradient-drift and current-convective instabilities) without definitive evidence, and (2) give consideration to other sources of plasma structure in blobs. Because MFTI acting on an existing plasma-density gradient is by far the most efficient process for producing strong irregularities, a first step is to consider other sources of irregular electric fields. Other sources include magnetospheric turbulence, E-region polarization effects, and field-aligned currents.

It seems clear, therefore, that we need to establish (1) whether MFTI from irregular electric fields is indeed a viable means of producing plasma structure along a blob wall, and (2) if so, whether those irregular electric fields are always generated by F-region

5

polarization effects. A direct means of determining whether an MFTI
process is operating to produce blob structure is to measure the
two-dimensional spatial pattern of plasma drift that accompanies a
structured plasma-density distribution. If MFTI is operative as a
structuring mechanism, there should be (1) different plasma-drift
velocities associated with lower and higher number-density regions, and
(2) relative motion such that high number-density regions move toward
low number-density regions, and vice versa. Finally, if F-region
polarization effects are responsible for the MFTI, the slip velocity
should be inversely correlated with plasma density.

The key distinction that makes the above requirements amenable to
experimental verification is the fact that those requirements are valid
regardless of the time history of observed plasma structure. It does
not matter what the original source of that structure was prior to
observation. The above requirements, therefore, can be used to verify
MFTI as an ongoing structuring process and to determine the presence or
absence (at the time of measurements) of F-region polarization electric
fields.

In this paper, we present the first results from an experiment
specifically designed to obtain the above information. (The total
experiment consisted of EISCAT incoherent-scatter measurements made
around the times of overpasses by the HILAT satellite [see Fremouw et
al., 1983]. HILAT measured precipitating particles, field-aligned
currents, electric fields and radiowave scintillations.) Using only
data collected with the tristatic EISCAT radar facility, we show that
MFTI was acting (during the observation period) on the poleward wall of
a blob to produce structure. (Detailed HILAT results will be reported
in a future paper.) Although the estimated growth rate appeared to be
rapid enough to have produced the observed structure in several minutes,
no strong claim is made for that conclusion. We show, however, that the
ongoing MFTI process could not have been controlled by F-region
polarization electric fields, and conclude ón that basis that neither
the gradient-drift nor current-convective instability was active during
the observation period. We suggest that the absence of F-region

6

polarization effects can be attributed to the presence of a highly
conducting E layer. More cases, however, need to be analyzed before we
can discount, in general, the role of F-region polarization electric
fields as a blob structuring mechanism.

In Section II, we describe the EISCAT radar experiment designed
to investigate the blob structuring process. The results are described
in detail in Section III and summarized in Section IV. Finally,
implications of the results are discussed in Section V.

II. THE EXPERIMENT

During a recent Swedish EISCAT campaign (24 February to 15 March 1984), three two-hour experiments were conducted to determine (1) blob structure in a plane transverse to the geomagnetic field and (2) the associated plasma-neutral dynamics. Each of the three experiments were centered on times of closest approach of HILAT, a satellite instrumented specifically for the investigation of F-region plasma-density irregularities [Fremouw et al., 1983]. Satellite pass times in the vicinity of the EISCAT radar facility varied between 2200 and 2230 UT. (Local solar time (LST) leads universal time (UT) by 1 h 28 min (± 2 min) at the center of the scanned sector.) Data were collected on 24, 25, and 29 February 1984. Geomagnetic activity was generally rather mild, with highest activity during EISCAT measurements on February 25, followed by those on February 24 and 29.

The objective of these experiments was to measure both the F-region plasma density and electric field locally, as a function of latitude and longitude. Because zonal convective flow usually dominates plasma motion in the auroral zone, we designed an antenna scan pattern so that longitudinal information could be inferred from the time-space conversion. (The radar mode of operation is described in following paragraphs.) In this sense, the approach is similar to that used by Tsunoda and Vickrey [1984]. The key difference from Tsunoda and Vickrey [1984] is that EISCAT is able to measure the local electric field vector, not simply the line-of-sight velocity. Measurement of the electric field vector allows us to test whether an MFTI process is operating or not. In addition, it is possible to determine the relative drift (or slip) velocity between ions and neutrals if we are able to estimate the neutral wind vector. Originally, it was our intent to utilize both EISCAT and a Fabry-Perot interferometer to provide F-region neutral wind measurements. Unfortunately, the skies were cloudy during the period of interest. For this reason, we have estimated the neutral wind from only incoherent scatter measurements. (The analysis technique is described later in this section.) Estimates of the slip velocity vector allow us to test whether F-region polarization effects are present.

8

A rapid, quasi-scan mode was implemented using the tristatic EISCAT radar facility so that local measurements of plasma density, electron and ion temperatures, and electric field could be made along a magnetic meridian at 300-km altitude. (The EISCAT system is described by Folkestad et al. [1983].) The scan geometry is shown in Figure 1. The scan consisted of 8 fixed positions spaced 0.25 deg in geographic latitude; the total coverage was approximately 65 to 67 deg in invariant latitude. The scan meridian is seen in Figure 1 to be displaced to the east of the Tromso-Kiruna meridian; the displacement was chosen to improve the signal-to-noise ratio (SNR) of the incoherent-scatter returns received at Sodankyla. The geometry also allows for comparable accuracies in the estimate of all three velocity components.

The radar measurements were made as follows. As the antenna was step-scanned from north to south, data were recorded for 25-s at each of the eight antenna dwell positions. The total scan cycle was 5 min 10 s, including the times to move between dwell positions. Two waveforms were used; a 200-μs pulsewidth (30-km range resolution) for monostatic reception at Tromso, and a 700-μs pulsewidth for bistatic reception at Kiruna and Sodankyla. (Note that in bistatic reception, the intersecting antenna beamwidths (0.6 deg) rather than pulsewidth determine range resolution.) Ten autocorrelation functions (ACF) were computed at Tromso, starting at 150 km range and at 30-km intervals. A single ACF was computed at each of the remote sites, centered at an altitude of 300 km.

For analysis, the data (recorded with 5-s on-line integration times) were post-integrated for the full 25-s of recording at each antenna dwell position. All ionospheric parameters were computed using the 64-lag ACFs. We note that plasma densities computed from ACFs include received-power corrections for temperature-ratio effects, and therefore represent best estimates of true plasma density. The ion velocity vector was determined from three line-of-sight measurements; that measured at range gate 7 at Tromso, and those measured at 300-km altitude by the remote sites. At this altitude, the ion velocity is essentially identical to that of bulk plasma drift (i.e., $\underline{E} \times \underline{B}/B^2$).

Because of the unavailability of F-region neutral wind measurements (due to cloudy skies) from the concurrently operated Fabry-Perot interferometer, we extracted neutral-wind estimates from incoherent scatter measurements. The technique for deriving the meridional component of the neutral wind has been described in detail by Evans [1971], Amayenc and Vasseur [1972] and Wickwar et al. [1984], and therefore, will not be repeated here. The technique basically consists of using measurements of plasma drift along geomagnetic field lines, correcting for ambipolar diffusion, and solving for the meridional wind; a horizontal wind is assumed to be responsible for field-parallel plasma motion through ion drag. Although actual field-parallel measurements are best for this purpose, the tristatic measurements used here provide reasonable estimates of field-parallel drift under conditions of small convection velocities. But more importantly, local ion velocity vector measurements allow us to compute the meridional neutral wind as a function of latitude. (We show in Section III that the mean convection velocities were indeed small.) Comparisons of radar-derived meridional neutral wind with Fabry-Perot interferometer measurements have shown very good agreement [e.g., Nagy et al., 1974; Rees et al., 1984; Wickwar et al., 1984].

Determination of the zonal component of the F-region neutral wind is considerably more involved than that for the meridionnal component. Bates and Roberts [1977b] have demonstrated that it is possible to estimate the zonal component from the ion energy equation. The energy equation requires knowledge of the ion and neutral temperatures as well as other components of the plasma drift velocity. If we assume electron heating to be zero and use a model value for the neutral temperature, we can solve a quadratic equation for the zonal neutral wind. (If we assume ion drag as the dominant coupling mechanism between ions and neutrals, the choice of the solution with smallest magnitude is reasonable.) Bates [1978] has shown that the model neutral temperature is a reasonable approximation, even during a heating event.

This technique has been refined and tested by Rees et al. [1984] and Haggstrom et al. [1984] on data taken simultaneously by EISCAT and a

10

630 nm Fabry-Perot interferometer. They have included electron heating of the ion gas and the effects of a bi-Maxiwellian distribution that occurs under conditions of large electric fields [e.g., St.-Maurice and Hanson, 1982]. Rees et al. [1984] and Haggstrom et al. [1984] found good agreement in both components of the neutral wind measured by the two techniques. Significant error in the radar estimate of the zonal neutral wind occurred only at times when there were large increases in the neutral temperature (both used the MSIS model values [Hedin et al., 1977] for the neutral temperature). The same analysis program utilized by Rees et al. [1984] and Haggstrom et al. [1984] have been used here to obtain estimates of the neutral wind vector. We show in Section III-A-4 that large increases in the neutral temperature seems not to have occurred during the event under study.

III. RESULTS

The results are presented in two parts. In Section III-A, we present an overview of magnetic and ionospheric conditions that occurred during the experiment. We then describe the temporal behavior of mean electrodynamic parameters (plasma drift, neutral wind, and slip velocity) associated with an isolated negative bay event that was centered in our observation period. Because of similarities found between the negative bay event and an auroral substorm [e.g., Gurnett and Akasofu, 1974; Lassen et al., 1977], we have ordered our results according to substorm phase. Similarity of our results with others should lend some confidence to our measurements on the basis of consistency. We find that the mean slip velocity (needed to drive the gradient-drift instability) was small during the growth phase but increased to large values with a generally poleward direction during the peak and recovery phases. Although we do not describe the blob of interest in any detail until the next section, we note the unfavorable conditions for ongoing structuring (via F-region polarization effects) along the poleward wall of a blob; i.e., on the basis of a poleward-directed slip velocity and the presence of a highly conducting E layer.

In Section III-B, we consider detailed spatial relationships between plasma and electrodynamic parameters to actually evaluate the roles of MFTI and F-region polarization effects during the measurement period. We present two-dimensional patterns (in a plane transverse to the geomagnetic field) of plasma density, velocities, and temperatures, and point out correlations (or their lack of) with one another. The blob of interest is described and shown to be characterized by plasma structure along its poleward wall. We show that plasma structuring by MFTI was occurring along the poleward wall but that MFTI was not being driven by F-region polarization electric fields. The absence of F-region polarization effects is attributed to the presence of a conducting E layer. The unambiguous existence of spatially (rather than temporally) irregular electric fields that may have driven the MFTI

12

process is demonstrated by examining the eastward component of plasma drift measured simultaneously at several closely-spaced longitudes. The fact that irregular electric fields existed in the absence of F-region polarization effects implies that the irregular electric fields must be driven by some other source than gradient-drift instability, such as magnetospheric turbulence, or E-region polarization effects.

A. Overview and Relationships Between Mean Plasma and Electrodynamic Parameters

   1. Geomagnetic Conditions and Mean Electrodynamic Drift

For an overview, we use magnetograms obtained at Kiruna, Sweden to characterize conditions during the experiment. (Cloudy skies prevented ground-based optical coverage for this period.) The period of interest is between 2100 and 2300 UT on 25 February 1984. The Kiruna magnetogram showed magnetically quiet conditions 6 hours prior to the experiment and 10 hours after completion of the experiment. This period of prolonged magnetic quiescence was interrupted by a single isolated negative bay, centered within the two-hour period of the experiment. The magnetic Kp index varied as follows: 0+ (1500 to 1800 UT), 1 (1800 to 2100 UT), 3 (2100 to 2400 UT), 0+ (0000 to 0300 UT), and 1 (0300 to 0600 UT) [Coffey, 1984].

An 8-hour segment of the magnetogram centered on the experiment is presented in Figure 2. The X, Y, and Z components of the magnetic perturbations correspond to geographic North, East, and vertically down directions, respectively. (Geomagnetic North is 12 deg west of geographic North.) The negative bay, seen in the X component, can be characterized by three phases: (1) a growth phase which started around 2100 UT, (2) a peak phase when the magnetic perturbation reached a maximum value of -130γ around 2140 UT, and (3) a recovery phase which lasted from 2200 UT to around 0030 UT. The negative bay is interpreted as being produced by a westward electrojet flowing in the auroral E layer. The positive Y component reflects the extent to which the westward electrojet direction was rotated south of geographic West. (Because of the 12 deg offset between geographic and geomagnetic

13

coordinates, a westward electrojet (in geomagnetic coordinates) would still produce a small positive perturbation in the Y component.) The negative Z component further indicates that the centroid of auroral current was situated poleward of Kiruna. Combining the X and Y components, we find that the maximum horizontal perturbation vector during the peak phase (at 2150 UT) was -170 γ, directed 28 deg east of geomagnetic South. (We compare this magnetic perturbation vector to the mean plasma drift velocity described below.)

From the overview, we find that a natural ordering of our observations could be by phases of the magnetic disturbance. We therefore proceed to describe the mean electrodynamic parameters in this framework.

The mean electrodynamic parameters were extracted from EISCAT data taken during 17 meridian scans, starting at 2115:42 UT (scan 1) and ending at 2242:12 UT (scan 17). We see from Figure 2 that this period essentially brackets the three phases of the negative bay event. The mean plasma drift velocity was computed by averaging drift velocities from the eight antenna positions in a given scan. Similar computations were made for the mean neutral wind and mean slip velocity. The three mean velocity vectors are presented as a function of scan number in Figure 3, with their azimuthal directions shown in the top panel and their magnitudes shown in the bottom panel. (Magnetic East is shown in the top panel by a horizontal line.)

The mean plasma drift velocity is seen to vary in concert with the phases of the negative bay event. The drift speed is seen in Figure 3 to decrease from 436 m/s in scan 1 down to 183 m/s in scan 2, before recovery to 394 m/s in scan 5. This temporary decline in drift speed is closely followed by a southward turning of the plasma drift vector (between scans 2 and 3). The southward turning of the drift velocity during the growth phase of the negative bay is similar to the development of a westward electric field during the growth phase of an auroral substorm [e.g., Gurnett and Akasofu, 1974; Rino et al., 1974; Lassen et al., 1977].

14

During the peak and recovery phases (scans 5 through 17), only the direction of mean plasma drift appeared to display substorm-related behavior. As its speed decreased more or less monotonically through this period, the plasma drift vector rotated from a southeastward direction back towards magnetic East (scans 9 to 11) and remained there throughout the recovery phase. The southeastward direction of the plasma drift vector therefore is identified with the growth and peak phases of the negative bay event, and a purely eastward drift is associated with the recovery phase.

Given the mean plasma drift in the F region and the magnitude of magnetic disturbance, we can estimate the conductance of the E region. At 2150 UT (during the peak phase), the drift velocity was 270 m/s directed at -50 deg south of geomagnetic West. For a magnetic perturbation vector that was -170 γ directed 28 deg east of geomagnetic South, the average current vector must have been directed 12 deg clockwise of the electric field vector. This implies that the Pedersen conductance was about 4.7 times greater than that of the Hall conductance. This ratio is extremely high and implies an average energy of precipitating electrons that is less than 1 keV [e.g., Spiro et al., 1982]. If we use an infinite current-sheet approximation, we obtain a Pedersen conductance of 20 mhos. This rough estimate is approximately a factor of two larger than peak values reported by others [e.g., Brekke et al., 1974; Vickrey et al., 1980, 1981; Wallis and Budzinski, 1981; Senior et al., 1982; Spiro et al., 1982].

From the above analysis, we are made aware that the E-layer Pedersen conductance was probably high (at least during the peak phase of the negative bay) and that F-region polarization shorting by a conducting E layer must be given due consideration. Somewhat more accurate estimates of the Pedersen and Hall conductances computed from plasma-density profiles obtained during the three phases of the magnetic disturbance are presented in Section III-A-4. With awareness that we are analyzing an event characterized by a highly-conducting E layer, we proceed in the next section to describe the neutral wind characteristics. Knowledge of the neutral-wind characteristics is

15

extremely important because it is the slip velocity, not plasma drift velocity, that acts to set up F-region polarization electric fields on plasma-density gradients.

    2. Mean Neutral Wind

    The mean neutral wind is seen in Figure 3 to display time-varying characteristics that are not always simply related to the plasma drift velocity variations described in the previous section. During the growth phase, the neutral wind tracked the plasma drift velocity very closely. Both the substorm-related, southward turning of the plasma drift vector and the temporary decline in speed are reflected in the neutral wind. This behavior implies (1) strong coupling of the neutrals to the plasma, and (2) the dominance of nearby convection electric fields over pressure gradients as the source of the neutral wind. Because the e-folding response time of neutrals to changes in plasma motion approaches an hour (for typical plasma densities) at 300 km altitude [e.g., Fedder and Banks, 1972], close tracking of the plasma by neutrals also suggests the absence (or relative ineffectiveness) of other transient or spatially-varying forces on the neutral gas during the prolonged period of magnetic quiescence that preceded substorm activity.

    The peak-phase onset was followed (within 10 minutes) by a substantial increase in the mean neutral wind speed, reaching 750 m/s during scan 7. (Note that the neutral wind direction remained unchanged during this surge.) The gust of neutral wind (which lasted until scan 10, or about 20 minutes) was not preceded nor accompanied by a locally-large plasma drift velocity. The wind source, therefore, was (1) situated around magnetic midnight, (2) located poleward of the EISCAT field of view, and (3) configured in the form of a narrow channel (or "throat") of large antisunward convection velocity (or heat source).

    The behavior of the mean neutral wind towards the end of the peak phase and the start of the recovery phase did not reflect the strong coupling to plasma drift seen during the growth phase. As the plasma drift vector changed from a southerly direction back toward magnetic

16

East, the neutral wind did not track the rotating plasma drift vector. Instead, the wind vector remained in a southerly direction. This behavior can be understood if we recognize that the ion-neutral interaction is not a reciprocal process. While the neutrals are freely moved (with a time constant of several tens of minutes) by plasma convection, the plasma cannot be moved across magnetic field lines by the frictional ion drag applied by a neutral wind. Therefore, without an F-region dynamo (i.e., a polarization electric field), the plasma will only move in a pattern dictated by the convection electric field. The neutral wind pattern, however, would be complex, and will reflect motion produced by plasma convection, pressure gradients, and inertial effects.

To assess the nature of the observations, we briefly review current understanding of F-region neutral winds seen in the midnight sector. A southward surge of the neutral wind in the midnight sector of the auroral zone appears to be a common feature [Nagy et al., 1974; Bates and Roberts, 1977a; Hays et al., 1979; Roble et al., 1982; Wickwar et al., 1984]. Because of its consistent occurrence around magnetic midnight, the southward surge does not seem to be necessarily substorm related. From observed characteristics, the above researchers have speculated that the source of the midnight surge is likely to be ion drag by antisolar convection in the polar cap. The high wind speed seen in our data without locally-large plasma drift is consistent with that hypothesis of neutral-gas acceleration in the polar cap. Antisunward convection has, of course, been observed over the polar cap [e.g., Heppner, 1972, 1977; Heelis and Hanson, 1980].

The wind speed in the midnight surge has also been shown to be related indirectly to the strength of the polar cap electric field. Bates and Roberts [1977a] have shown that the logarithm of wind speed is directly proportional to the magnetic Kp index. For Kp = 3 (i.e., conditions during the experiment), a wind speed of 770 m/s would be predicted by their empirical relationship. Our measured wind was 750 m/s, in excellent agreement with that prediction. This agreement tends to lend some credence to the extremely large neutral wind speed reported

17

here. As further support, however, a wind speed of 750 m/s is actually comparable to other estimates of maximum neutral wind obtained by both incoherent scatter radar and Fabry-Perot interferometer [V. B. Wickwar, personal communication, 1985].

While the onset time for southward neutral wind is expected to occur sometime around magnetic midnight, we believe that the commencement of the midnight surge within 10 minutes of substorm onset was coincidental. We speculate that the interplanetary magnetic field (IMF) was directed northward during the 6 hours of magnetic quiescence prior to the substorm, thus resulting in a small polar cap electric field. We further speculate that the IMF turned southward, followed by an increase in electric field strength. The substorm onset followed the development of the polar cap electric field. The apparent 10-minute lag in neutral wind surge from substorm onset is not likely to be associated with onset, but more likely to be associated with the time necessary to accelerate the neutrals in the polar cap and for the neutral wind to propagate into the EISCAT field of view. If we assume that the wind maintained a speed of 750 m/s, the wind acceleration region would have to be placed around four deg north of EISCAT, i.e., around 70 deg invariant latitude. Although this latitude is not unreasonable as the location for the polar cap boundary, we suspect that the acceleration region was situated further to the north; on this basis, the neutral-wind acceleration process would have begun prior to substorm onset. The above scenario is based on similar observations in separate case studies by Gurnett and Akasofu [1974] and Lassen et al. [1977]. In their case study, Gurnett and Akasofu [1974] showed that the polar cap electric field developed at least 28 minutes after the southward turning of the interplanetary magnetic field (IMF) and that substorm onset occurred at a time when the electric field was already large.

Using the above scenario as a working hypothesis, we can further speculate that the width of the midnight surge (in local time) may also be related to magnetic activity. Wickwar et al. [1984] have presented data in which the width of the surge varies from 1 to 3 hours, and appears to be a function of magnetic activity. Because of magnetic

18

quiescence that occurred both before and after our negative bay event, it does not seem unreasonable to expect a minimal width, perhaps as narrow as 20 minutes. Convection patterns now being proposed to represent northward IMF conditions [e.g., Potemra et al., 1984] contain a feature that resembles a narrow channel of antisolar convection.

An alternate explanation, however, for the short-lived gust in neutral wind seen during scan 7 might be the transient occurrence of a vertical wind. Bates and Roberts [1977a] and Wickwar et al. [1984] have suggested that at least some of the apparently-large surges in the meridional neutral wind (estimated from incoherent scatter observations) may be produced by atmospheric gravity waves. The notion of gravity-wave influence on computed winds might be supported by the recurrence of another peak in wind speed during scan 13 (see Figure 3). If this is the case, an atmospheric gravity wave could produce a vertical wind component that is mistakenly assumed to be a component of a horizontal wind.

The possibility of gravity-wave contamination of our neutral wind estimates seems to be discounted by the temporal behavior of the F-layer peak in plasma-density profiles obtained with EISCAT. We show in Section III-A-4 that the F-layer peak altitude moved upward with development of the southward surge. More importantly, upward movement of the peak altitude occurred simultaneously over several degrees of latitude. The widespread lifting of the F layer is more in agreement with a southward neutral wind than the passage of an atmospheric gravity.

The observed modulation of the neutral wind speed may be explained by braking action imposed on the neutrals by oppositely convecting plasma. In particular, neutral-wind variations seen in Figure 3 may be explained by (1) the onset of southward surge in neutral wind (driven by a source poleward of the EISCAT field of view), and (2) by modulation of the southward neutral wind by a substorm-related turning of the plasma drift vector. When the drift vector returned to an eastward direction, it no longer contributed to the modulation of the southward neutral

19

wind. This question of dynamic interaction between neutrals and plasma
is also crucial to the production of plasma structure by F-region
polarization electric fields.

3. Slip Velocity

The dynamic interaction of plasma with neutral gas during this
period is best described by the slip velocity vector which is also
plotted in Figure 3. As might be expected from the above description,
the slip speed was small prior to scan 5, during the growth phase. The
slip speed increased rather abruptly during scan 7, produced by a large
southward surge in neutral wind. The slip speed remained above 250 m/s
during the remainder of the scans, with relative maxima occurring in
scans 7 and 13. Throughout this period, the slip velocity vector was
directed towards magnetic Northeast.

From the described behavior of the mean slip velocity, we can draw
some conclusions regarding the expected plasma structuring process. If
we assume a blob that is elongated in longitude, the gradient-drift
instability could only be weakly operative prior to scan 5, during
growth phase. The large poleward-directed slip velocities that existed
during peak and recovery phases would predict structuring (damping)
along the equatorward (poleward) wall of a longitudinally elongated
blob. The above scenario, of course, applies only in the absence of a
highly-conducting E layer.

Having demonstrated that the mean slip velocity was large during
the peak and recovery phases of the substorm, we would like to determine
whether E-layer Pedersen conductance remained high throughout this
period. We do so in the next section.

4. Plasma Density Profiles

The analysis up to this point has focused on characteristics of
mean electrodynamic parameters. We also require some knowledge of the
plasma parameters, i.e., plasma density, electron and ion temperatures.
For example, we have made only a crude estimate of E-region Pedersen
conductance, and that only during the peak phase of the substorm. It is

20

therefore desirable to have other estimates of E-region Pedersen conductance, especially as a function of substorm phase. Also because of the importance of neutral wind characteristics to the conclusions to be drawn in this paper regarding F-region polarization effects, it is desirable to cross-check those measurements wherever possible. In this vein, we examine the altitude behavior of the F-layer peak. The peak altitude is sensitive to the meridional neutral wind. And, there is also the question regarding F-region plasma structure production by other means than MFTI, such as structured soft particle precipitation. We therefore examine representative profiles of the plasma parameters to shed some light on some of these questions. (Elevated electron temperatures as indicators of soft particle precipitation are discussed in the next section.)

The plasma density profiles measured at Tromso during scans 1, 7, and 17, are presented in Figure 4. The abscissas scale for each set of profiles is referenced to a nearby vertical line that corresponds to 10^5 el/cm^3 for that data set. Although these profiles were obtained along non-vertical lines of sight from Tromso, they are useful as general descriptors of plasma density distribution in altitude. We use profiles from scan 1 as representative of the growth phase, those from scan 7 as representative of the peak phase, and those from scan 17 as representative of the recovery phase.

We first use the plasma density profiles to determine the morphology of keV electron precipitation. Morphological description, in this case, is limited to a narrow range of latitudes covered by the E-region penetration points of the Tromso beam during meridian scans. Referring to Figure 1, latitudinal coverage of the eight E-region range gates corresponds to that for scan positions 1 to 4 at 300-km altitude. During the growth phase (scan 1), E-layer plasma densities ranged from 1.5×10^5 el/cm^3, to as little as 9×10^4 el/cm^3. Examining individual profiles, we find a latitudinal increase in plasma density with decreasing latitudes; we do not know if the gradient is spatial or temporal. During the peak phase (scan 7), E-region plasma densities reached 3.5×10^5 el/cm^3, more than double that seen in scan 1 and

21

indicating increased particle precipitation. Again, there is
variability in the latitudinal pattern. (Evidence of auroral arcs were
not found within the EISCAT field of view in HILAT data.) And during
the recovery phase (scan 17), the E-region profiles were relatively well
behaved with a peak value of 4×10^5 el/cm^3, indicating little if any
reduction in precipitation from that seen during the peak phase.

From the above, we can reconstruct the auroral process associated
with the substorm. The relatively high plasma drift during growth and
early peak phases suggests that negative bay onset was probably produced
by an abrupt increase in particle precipitation, not an enhancement in
convection velocity, in agreement with other observations of this kind
[e.g., Gurnett and Akasofu, 1974]. The recovery phase appears to have
been associated with a gradual decrease in mean convection speed, and
not by a reduction in the number flux of keV electron precipitation.
The evidence indicates that E-layer-producing precipitation remained
relatively uniform during the peak and recovery phases of the substorm.

To augment our single crude estimate of E-region Pedersen
conductance (Section III-A-1), we present other estimates based on the
plasma density profiles in Figure 4. Because the peaks of E layer
profiles were not measured, we simply matched our peak plasma density to
one in Figure 10 of Vickrey et al. [1981] to estimate the Pedersen
conductance. (This approach is not unreasonable because we have
measurements of plasma density as low as 118 km altitude; the largest
contribution to Pedersen conductance comes from 125 to 130 km altitude.)
We obtain a peak value of about 8 mhos for scan 7. The Pedersen
conductance was found to be one-half that of the Hall conductance (much
smaller than that estimated from magnetic records). If we further
assume that the profile shape does not significantly alter the Pedersen
conductance, the conductance should scale as the plasma density. With
this as a basis, we found that the Pedersen conductance varied from 2
mhos during the growth phase to 8 mhos during the peak and recovery
phases. These values are still large compared to a typical F-layer
Pedersen conductance of 0.1 mho [Vickrey et al., 1980].

22

Next, we introduce the blob of interest, as it appears in plasma density profiles and in comparison to the background ionosphere. (Structure associated with the blob is described in Section III-B.) The blob is seen in plasma density profiles from scan 7. The blob corresponds to the two most enhanced F-layer plasma densities, reaching a value of 3.3×10^5 el/cm^3. The other F-layer profiles in scan 7 represent the background ionosphere poleward of the blob, measured during the peak phase of the substorm. The peak altitude of the blob is around 300 km. In comparison, F-layer profiles from scan 1 represent the background ionosphere, also poleward of the blob but measured during the growth phase. The peak plasma densities from scan 1 are slightly higher than those background measurements in scan 7. The F-layer peak in scan 1 is seen to be below 300 km altitude. The third set of profiles in Figure 4 correspond to the background ionosphere equatorward of the blob, measured during the recovery phase. Peak plasma densities are seen to approach those in the blob. The most striking feature, however, is the altitude of F-layer maximum, reaching at least 350 km. The profiles are also characterized by their similarity in shape and number density.

The lower background plasma densities found in scan 7 compared to scan 1 may have resulted from enhanced electron loss rates initiated by the large slip velocities that occurred during the peak and recovery phases. Banks et al. [1974], Schunk and Banks [1975], and Schunk et al. [1976] have shown that large electric fields lead to ion composition changes that enhance the electron loss rate.

The increase in F-layer peak altitude is consistent with the presence of a southward neutral wind. Watkins and Richards [1979] have shown that a 400 m/s neutral wind, when directed equatorward, lifts the peak of the F layer from 300 km to 380 km altitude. The actual displacement of course depends on the length of time that the neutral wind has been applied (90 minutes in their example). Their modelling results are in good agreement with our neutral wind results in Figure 3 and plasma-density profiles in Figure 4. (Examining other plasma density profiles, we found that the F-layer peak was already located

around 340 km by scan 11, i.e., end of the large southward surge in neutral wind.) We therefore conclude that a substantial equatorward-directed neutral wind was indeed present during the peak and recovery phases of the substorm.

Finally, we address the question of soft particle precipitation as an ionization source. We use plasma densities measured between 150 and 200 km altitude as a measure of softer electron precipitation. Loss rates in this altitude range are still rapid enough that the plasma density distribution reflects production rates and not transport effects. Examining profiles in Figure 4, we find a precipitation morphology that differs from the harder keV electron precipitation responsible for the E layer. The plasma density (at say, 200 km altitude) is seen to have increased from scan 1 to scan 7, as expected. The plasma density, however, decreased substantially from scan 7 to scan 17; the decrease is to values less than found during scan 1. This difference in precipitation morphology at the two altitudes is also manifested in Figure 4 as a change in the slope of the topside E layer profile. The altitude-dependent change in production rate suggests a change in the energy spectrum of precipitating particles. If the slope of the energy spectrum did change, it could be related to magnetic activity or to a viewing of a different region of the magnetosphere by the radar. This latter speculation suggests that the blob may have been located near a magnetospheric boundary that separates two particle populations. Further discussion of this possibility is presented in Section V.

The impact of even softer electron precipitation in producing plasma density at altitudes above 200 km is much less. At 300 km altitude, the e-folding ionization rate is greater than an hour [e.g., Roble and Rees, 1977; Watkins and Richards, 1979; Weber et al., 1984]. In this convection dominated region, a variety of plasma density profiles are found. Although the highest plasma densities are found in scan 7, some of the lowest values are also found during that scan. The profiles in scan 17 are characterized by their similarity in shape and value to one another, indicating a uniform plasma density distribution

24

at any given altitude. One possible interpretation of this last observation is that the region poleward of the blob is more irregular in plasma density distribution than that equatorward of the blob.

   5. Plasma Temperature Profiles

Because it is virtually impossible to detect the occurrence of soft particle precipitation at these altitudes from plasma densities, we turn to an analysis of plasma temperatures. Roble and Rees [1977] have shown that electron temperature peaks with the ionization rate, with a time constant of 10 s or less; and begins to decay only after the plasma density has become significant, i.e., on the order of 10^3 s. The situation, of course, is not so simple if precipitation occurs in the presence of significant existing plasma density. We can at least argue that, for a given plasma density, elevated electron temperatures imply ongoing or very recent precipitation, whereas low or normal temperature may or may not be associated with precipitation. Typical electron temperatures produced by soft-particle precipitation range from 2000 K to 3250 K [Roble and Rees, 1977].

The degree to which electron temperature is elevated by particle heating can be estimated by comparing the electron temperature at a given altitude to the corresponding ion temperature. The ion temperature profiles are presented in Figure 5. Except for some scatter in the profiles from scans 1 and 17, the ion temperatures are similar, all approaching an asymptotic value of about 1000 K at the highest altitudes. (The large increases in ion temperatures around 340 km altitude in scan 7 are not thought to be real.)

The electron temperature profiles are presented in Figure 6. Keeping in mind that the asymptotic value for the ion temperature was 1000 K, we notice that the electron temperature is considerably enhanced. The enhancements occurred above 220 km altitude and are evident in all profiles, including those obtained during the growth phase. The most dramatic variation occurred in scan 7 where there appears a distinct gradient in electron temperature. The highest temperatures occurred at the north end of the scan; the temperatures

25

decreased rapidly, reaching a minimum within the blob. On the other hand, the behavior of electron temperature in scan 17 is most like the ion temperature profiles. The electron temperature in scan 7 is about 500 K greater than those seen during scan 17.

The electron temperatures presented in this section clearly indicate soft particle precipitation in the region poleward of the blob, particularly during the peak phase of the substorm. Whether soft precipitation occurred within the fingers of the blob is investigated in Section III-B-4.

B. Relationships Between Plasma Density, Plasma Motion, Electron and Ion Temperatures

In Section III-A, we presented an overview of the substorm event being analyzed in this paper, and described the mean electrodynamic parameters. Selected profiles of plasma parameters were also presented to characterize the morphology of particle precipitation. From the analysis, we found that the E-region Pedersen conductance was high and that the slip velocity was directed poleward. In the absence of a conducting E layer, this slip velocity would predict the poleward wall of a blob should be stabilized by the gradient-drift instability.

In this section, we present an analysis of more detailed spatial relationships between two-dimensional patterns of plasma parameters and electrodynamic parameters, at 300-km altitude. From the analysis, we demonstrate that plasma along the poleward wall was being structured by MFTI but that F-region polarization effects were not operative. We argue that the rate of MFTI could have produced the observed structure along the poleward wall of the observed blob, if that rate were sustained for several minutes.

1. Plasma Density

A two-dimensional map of the plasma density measured at a nominal altitude of 300 km is presented in Figure 7(a). The distribution of plasma density is illustrated by isodensity contours and plotted in geomagnetic coordinates. Adjacent contours represent a change in plasma

26

density of 2×10^4 el/cm^3. Geomagnetic North is directed along the
ordinate and geomagnetic East is directed along the abscissas. The
ordinate scale of approximately 28 km between tick marks corresponds to
the spacing between scan dwell positions. The abscissas scale of about
67 km between scans (i.e., tick marks) is based on an average eastward
drift of 220 m/s measured during the 17 meridian scans. For discussion
purposes, we have superimposed unit vectors that represent the
directions of the slip velocity over the contours of plasma density.

The plasma-density contours shown in Figure 7(a) were constructed
from Tromso incoherent-scatter measurements at range gate 7. The
altitude for that range gate varied from 316 km at the north end of the
scan to 263 km at the south end of the scan. The altitude is about 300
km at the center of the scan. In addition, the upward movement of the F
layer (shown in Figure 4) produced by a large southward neutral wind,
however, did act to gradually decrease the overall plasma densities at
around 300-km altitude in the later scans. Fortunately, the basic
structural pattern shown in Figure 7(a) was not significantly distorted
by the gradual altitude change of range gate 7 nor by the lifting of the
F layer. The scan numbers can be converted to approximate times by
noting that scan 1 started at 2115:42 UT and that each scan takes about
5 min 10 sec to complete. Other start times for scans discussed below
are 2141:32 UT (scan 6), 2157:02 UT (scan 9), 2207:22 UT (scan 11), and
2238:22 UT (scan 17).

The feature of interest in Figure 7(a) is the region of enhanced
plasma density outlined by the 2×10^5 el/cm^3 contour (i.e., the most
lightly shaded regions). The shape of this region (outlined by a heavy
contour line), which we define as that of the blob, can be characterized
as follows. The general blob pattern was tilted with respect to the
geomagnetic east-west direction, and visible in 12 successive scans.
Using the average eastward drift speed of 220 m/s, the blob pattern can
be thought of as being elongated in longitude and extended over 750 km.
The most interesting blob features are the pronounced spatial
undulations of the 2×10^5 el/cm^3 (heavy line) contour along the
poleward wall of the blob, and the very shallow modulation along the

27

equatorward wall. The modulation depth along the poleward wall is about 80 km. Except for its location along the poleward (rather than equatorward) wall of the blob, the east-west structure is similar to that reported by Tsunoda and Vickrey [1984]. For the estimated 67-km interval between scans, we obtain an average spacing between the enhanced plasma protrusions, or "fingers," of about 200 km. Tsunoda and Vickrey [1984] found fingers along the equatorward wall of their blob with a finger spacing of about 150 km.

Besides spatial undulations in the 2×10^5 el/cm^3 contour, we find that the peak plasma density within the blob varied as a function of longitude, or time. The variation occurred primarily during scans 6 through 9 with peak plasma density reaching a value of 3.3×10^5 el/cm^3. These scans were made between 2141:32 and 2200:52 UT, during the peak phase of negative bay activity. These enhanced plasma densities were also seen in Figure 4 and pointed out in Section III-A-4 to be time coincident with substorm-related precipitation. Although we defer the question of ionization production by soft particle precipitation to Section III-B-4, we emphasize that we are concerned here with only the existing plasma-density distribution. (It is beyond the scope of this paper to attempt to account for the past history of sources responsible for observed blob structure.)

We estimate the ratio of plasma density found within the blob to that between the fingers, and also to that in the background ionosphere. Background plasma densities were as low as 1.0 to 1.3×10^5 el/cm^3, as found for example in the lower left hand corner and upper right hand corner in Figure 7(a). The plasma density between the fingers was a little higher than the background ionosphere, about 1.8×10^5 el/cm^3. From these rough estimates, the blob-to-background ratio in plasma density was about 1.3 to 1.7. In comparison, Tsunoda and Vickrey [1984] found ratios greater than a factor of 4.

From the brief discussion at the end of Section III-A-3, the plasma density distribution in Figure 7(a) seems to be inconsistent with the hypothesis that the gradient-drift instabilty was responsible for the

28

observed structure. We recall that the mean slip velocity was directed poleward and therefore that velocity would be expected to reduce any existing structure by the gradient-drift instability (for the same reason that structure growth would be expected along the equatorward wall of the blob). We also have found that the ratio of blob plasma density to that of the background F layer was small, and that the E-layer Pedersen conductancve was high during the period of negative bay activity. The results up to this point, of course, says nothing about how the observed plasma structure was produced, nor whether the structure was produced during the observation period or at some time in the past.

2. Ion Velocity

The conclusions drawn in the previous section can be taken a step further by analyzing the two-dimensional pattern of the plasma drift (or ion) velocity vector. While recognizing that we cannot unambiguously identify all contributing sources to the observed plasma structure along the poleward wall of the blob (without knowing its time history), we can determine (1) whether MFTI was occurring between high- and low-number-density plasma during the observation period, and (2) if so, whether the gradient-drift process was acting at that time to dampen the growth of plasma structure along the poleward wall.

The transverse component of the ion (or plasma drift) velocity vector is displayed in Figure 7(b). The velocity pattern is seen to be structured; the scale of velocity variations appears comparable to those in the plasma-density contours, suggesting a degree of coherence between patterns. At the largest scales, we find high ion velocities poleward of the blob. Velocities were generally greater than 400 m/s, except in the central portions of the first two scans where velocities were as low as 126 m/s. A peak velocity of 1122 m/s was observed at the north end of scan 3, just poleward of the smallest velocities. (Additional evidence of high velocities poleward of the blob is presented in Section III-B-5.) Velocities within and equatorward of the blob were generally between 100 and 300 m/s, although there are some localized regions of larger velocities (up to 600 m/s).

At scales on the order of the blob fingers, we find two regio... of large ion velocity that appear to be well correlated with the "depleted" plasma regions between fingers. Large velocities were observed primarily during scans 4 and 7. These velocities are seen to be directed southward, whereas velocities within the blob are smaller and directed slightly more eastward. For example, the blob velocity in scan 7 is 215 m/s while the depleted region is directed into the blob at a velocity of 534 m/s. The velocities associated with fingers are very similar to that found within the rest of the blob.

These observations of relative plasma motion between high- and low-number-density regions represent direct evidence of ongoing plasma structuring via an MFTI process. For example, the southward-directed depleted region in scan 7 must force the blob to distort its configuration in a manner to preserve incompressibility of the plasma. The depleted plasma will therefore push its way into the more dense plasma region resulting in longer fingers. This is, by definition, the MFTI process by which plasma is structured. The e-folding growth time for the finger in scan 6 is roughly estimated to be about 6 minutes (or equivalently, a growth rate of 3×10^{-3} s^{-1}).

There remains the question of space-time ambiguity. That is, the electric field could be time varying in a manner that results in the pattern observed. Doubt regarding our interpretation that might be cast by this ambiguity question is reduced by considering two points. First, the apparent spatial anticorrelation found in Figure 7 consisted of two high-velocity, low plasma density regions, and three low-velocity, high plasma density regions. We feel that the repetition of the anticorrelated patterns is more likely to be spatial than temporal. For example, if the poleward wall of the blob was actually smooth and time-varying east-west electric fields were responsible for the apparent modulations seen from scan to scan, we would expect (1) the equatorward wall to be similarly modulated as the poleward wall, and (2) the YO component of the Kiruna magnetogram should contain temporal oscillations. Neither is seen in the data. And second, we present additional velocity measurements in Section III-B-5 that demonstrate

unambiguously the existence of longitudinal variations in plasma drift velocity, consistent with the MFTI process. (Irregular electric fields were also measured by HILAT, and will be reported in a future paper.)

The spatial anticorrelation found between plasma density and ion velocity, and the sense of relative motion between high and low density plasma is not only direct evidence for the MFTI process, but also demonstrates the relative ineffectiveness of F-region polarization effects during this period. As pointed out earlier, the mean westward Pedersen current that is driven by the northward-directed slip velocity (see Section III-A-3), should act through F-region polarization electric fields to dampen structure development along the poleward wall of a blob. In other words, if the gradient-drift instability process was operative during the measurement period, the relative motion of high- and low-number-density plasma should be opposite in sense to that shown in Figure 7(b). This contradiction in the sense of relative plasma drift is strong evidence that F-region polarization electric fields did not develop (e.g., because of short-circuiting by a conducting E layer), or that MFTI was driven by other stronger electric fields that dominated over F-region polarization effects.

The presence of F-region polarization electric fields becomes even more doubtful when we compare the velocity pattern with plasma density distribution in scans 10 to 15. Rather than finding anticorrelation between the two quantities, we find a certain degree of correlation. For example, the ion velocity associated with the finger in scan 11 is 835 m/s and directed poleward, at an angle nearly perpendicular to the blob major axis. At the same time, we find velocities between 78 and 196 m/s in the depleted regions adjacent to the finger.

Another piece of evidence against the importance of F-region polarization electric fields is the occurrence of very large ion velocities in the upper right hand corner of Figure 7(b). Polarization electric fields are set up by charge accumulation along gradients in plasma density, in the presence of current flow. It is clear from Figure 7(a) that there were no significant plasma-density gradients in

31

the vicinity of those large observed velocities. From the above discussion, we conclude that F-region polarization electric fields could not have been responsible for the ongoing structuring by MFTI. Additional proof is presented in the next section.

3. Slip Velocity

While observed relative streaming between enhanced and depleted plasma regions represented ongoing structuring via the MFTI process, the slip velocity pattern in relation to the plasma-density pattern provides a true measure for the effectiveness of F-region polarization electric fields. In other words, if F-region polarization effects were operative during this period, we should find spatial anticorrelation (similar to that found between plasma density and ion velocity) between plasma density and slip velocity.

The slip velocity pattern is presented in Figure 7(c). We note that the striking anti-correlation found between plasma density and ion velocity, particularly between scans 3 and 9, is no longer as evident when the plasma density pattern is compared to that for the slip velocity. For example, the enhanced ion velocities measured between fingers during scans 4 and 5 are replaced by much smaller slip velocities (also see Figure 3). In the region between scans 6 and 8, the slip velocities remain enhanced but were directed poleward, rather than equatorward as in the case for ion velocities. (This spatial comparison of slip velocity direction with blob plasma density is facilitated by superimposing the directions of the slip velocity onto Figure 7(a).) This absence of inverse correlation between the two patterns is further evidence that F-region polarization effects were absent.

Finally, a poleward directed slip velocity should (in the absence of a conducting E layer) render the equatorward wall of a blob unstable to the gradient-drift process. From the shallow undulations in plasma density along the equatorward wall and the small ion (and slip) velocities found there, we would have to conclude that the gradient-drift growth rate must have been quite small.

32

4. Electron and Ion Temperatures

The electron temperatures computed from Tromso ACF data at range gate 7 are plotted in Figure 8(b). The temperatures ranged from 1380 K to 3007 K. On the largest scale, we see that elevated electron temperatures (> 2200 K; i.e., shaded regions) were confined to regions poleward of the blob (see Figure 8(a)). Typical temperatures in that region ranged from 2600 K to 2800 K. In comparison, the mean temperature within the blob in regions where the plasma density exceeded 2.8×10^5 el/cm^3 was 2000 K. Electron temperatures in less dense regions of the blob were between 1600 K and 1800 K. In comparison, the electron temperature in the background ionosphere ranged from 1400 K to 2000 K. The regions where most energy was deposited (at 300 km altitude) by particle precipitation, therefore, appears to have occurred poleward of the blob and in the highest-plasma-density region of the blob (between scans 5 and 10).

On scale sizes comparable to those of the fingers in Figure 8(a), we find that elevated electron temperatures occurred in the vicinity of the finger tips. The electron temperatures in fingers observed during scans 3, 6, 8, and 11, were 2100 to 2350 K, 2450 K, 2300 to 2400 K, and 2200 to 2500 K, respectively. These electron temperatures are higher by 100 to 500 K than that in the highest plasma-density region of the blob, and higher by 200 to 400 K than those in less dense portions of the blob. On this basis, enhanced soft-particle precipitation seems to have occurred at the tips of the fingers.

Some caution, however, must be exercised when we attempt to infer any increase in plasma density produced by soft particle precipitation. The regions of highest electron temperatures are not usually spatially coincident with regions of largest plasma density. For example, we find the highest electron temperature at the top of scan 7 to be in a region of very low plasma density. So, it is conceivable that the plasma was all at the same temperature at some time but cooling was slower where the electron density was low.

33

The ion temperature is of some interest in this kind of investigation because it is proportional to the square of the slip velocity. The slip velocity, together with the horizontal gradient in plasma density, control the development of F-region polarization electric fields. The use of ion temperature for this purpose, however, is not straightforward because the ion temperature is also proportional to the plasma density. Despite the complexity in interpretation, we include ion temperature for completeness.

The ion temperature was computed together with electron temperature, from the Tromso ACF data in range gate 7. The ion temperature, presented in Figure 8(c), ranged in value from 710 K to 1325 K. On the largest scale, elevated ion temperatures appear to occur outside the blob region of highest plasma density. Because plasma density is highest there, the ion temperature should be most sensitive to the slip velocity in that region. The finding of lowest ion temperatures in the densest portion of the blob indicates the presence of smallest slip velocities.

5. Additional Evidence of Spatially Irregular Electric Fields

In Section III-B-2, we raised the question of whether the irregular electric fields (or ion velocity) presented in Figure 7(b) were produced by spatial or temporal variations. Although the velocity variations from one scan position to the next is less likely to be temporal than those observed from one scan to the next, some doubt can reasonably exist. For this reason, we present additional evidence that unambiguously demonstrates the presence of spatially irregular electric fields.

For this purpose, we examined the line of sight velocities measured from Tromso whenever the antenna was fixed at scan position 1. The line of sight from Tromso was directed towards magnetic East, thus allowing measurements of the eastward component of plasma drift. Spatial information was obtained by plotting the eastward drift measured in the last 9 range gates. Of these, all but the first were at altitudes above 165 km and therefore provide a measure of the $\underline{E} \times \underline{B}$ plasma drift

34

velocity. For an elevation angle of 72.9 deg, the range gates were spaced at 8-km intervals in ground distance, starting 52 km east of Tromso. Any variation found in velocity as a function of range gate therefore represents a true spatial variation, averaged over 25 seconds.

The eastward plasma drift speed obtained as a function of range gate is presented in Figure 9. Velocity estimates from the 9 range gates are connected by line segments. Total ground coverage by these 9 gates is 64.7 km. Successive scans are plotted next to each other, with each scan separated from one another by a long tick mark. We note that these velocities are measured at the top edge of the two-dimensional maps in Figures 7 and 8.

We find that the velocity varied substantially during scans 1 through 7 and much less so thereafter. During scan 1, we see a velocity reversal in which an eastward drift of 500 m/s became a westward drift of comparable speed, over a ground distance of about 30 km. The westward drift slowly decreased during scans 2 and 3, reversing to an eastward drift in scan 4. Large eastward velocity spikes are seen during scans 3, 4, 6, and 7. The fractional velocity errors associated with these measurements all suggest that these large velocities are probably real, although those seen in scans 6 and 7 are the most convincing. Amidst these large velocity variations, we also find periods of relative calm, e.g., scans 2 and 5. From scan 8 on, we find a relatively well behaved eastward drift of about 500 m/s.

The amplitude of velocity fluctuations appears to be (1) larger poleward of the blob than equatorward of it, and (2) larger during the peak phase of the substorm than during the recovery phase. The first conclusion is based on comparisons of velocity fluctuations found in scans 1 through 7 to those in scans 11 through 17. In particular, the velocity fluctuations in scan 1 which occurred at the start of the growth phase was much larger than those in the later scans. A preliminary examination of electric field measurements made by HILAT also appears to support this observation. The second conclusion is apparent from Figure 9. The large velocity variations seen in scans 3

35

through 7 appear to be consistent with the vector velocities shown in Figure 7(b). The large spikes in Figure 9 occurred only during a period when there existed large vector velocities. The appearance of the spikes is consistent with simple rotation of the velocity vector as a function of longitude.

Because the plasma is incompressible at F-region altitudes, any longitudinal gradient in eastward plasma drift must be accompanied by a corresponding latitudinal change in northward plasma drift. But, because the longitudinal gradient in eastward drift was varying with longitude, we conclude that there was also a longitudinal gradient in the northward drift. On this basis, we conclude that there existed eddy-like turbulent flows with a scale size on the order of tens of km. The presence of a horizontal plasma density gradient in this irregular electric field pattern will result in plasma structuring by the MFTI process.

We note in passing that irregular electric fields have been observed in the past [e.g., Haerendel et al., 1969; Cauffman and Gurnett, 1972; Gurnett, 1972; Heppner, 1972, 1977; Aggson and Heppner, 1977; de la Beaujardiere and Heelis, 1984; Saflekos et al., 1985]; however, in most of those observations, the irregular electric fields were observed as a function of latitude.

IV. SUMMARY OF RESULTS

We have obtained the following results:

(1) An F-region plasma-density enhancement, or blob, was found around magnetic midnight in a zone of eastward convection;

(2) The two-dimensional spatial pattern of the blob (in a plane transverse to the geomagnetic field at 300 km altitude) was found to be elongated in longitude with substantial structure along its poleward wall;

(3) Structure along the poleward wall appeared in the form of four finger-like protrusions with an average length (or north-south modulation depth) of 80 km, and an average east-west spacing between fingers of about 200 km;

(4) Relative plasma motion was measured between enhancements and depletions in plasma density, providing direct evidence of ongoing plasma structuring by the MFTI process;

(5) Spatially-irregular north-south electric fields were measured as a function of longitude, indicating on the basis of plasma incompressibility that there also existed a corrsponding variation in the east-west electric field (i.e., that responsible for the MFTI);

(6) Mean plasma-electrodynamic conditions indicated that any plasma structure that existed along the poleward wall of the blob should have been in the process of being damped by the gradient-drift instability, a result that implies (when combined with result (4)) the absence of F-region polarization electric fields during the observation period;

(7) The slip velocity was not anticorrelated with plasma density, a result that also argues against the presence of F-region polarization electric fields;

(8) Estimates of Pedersen conductance in the E and F layers indicated that E-region current closure and the low ratio of Pedersen conductance between blob and background ionosphere could easily account for the absence of F-region polarization electric fields;

37

(9) Evidence against the presence of F-region polarization electric fields implies the ineffectiveness of both the gradient-drift and current-convective instabilities in this data set; and

(10) Soft-particle precipitation, as inferred qualitatively from electron temperature measurements, appeared to be most intense poleward of the blob with perhaps some precipitation occurring in the blob.

V. DISCUSSION

The major finding of this paper is that the fingers (particularly
that seen in scan 6) along the poleward wall of a blob were shown to be
participating in an ongoing plasma structuring process involving MFTI,
but that the MFTI was not driven by F-region polarization electric
fields. We presented direct evidence that there was relative motion
(produced by irregular electric fields) between adjacent regions of high
and low plasma density (along the poleward wall of the blob);
furthermore, the sense of that motion was consistent with ongoing plasma
structuring via MFTI. Although the estimated growth rate was found to
be high enough to have produced the observed fingers within several
minutes, whether it did or not is not the issue in this paper. We have
simply demonstrated that there can exist MFTI that can rapidly structure
a blob. Only the temporal persistence of a spatially irregular electric
field pattern has not been addressed.

The conclusion that F-region polarization effects were absent
during the observation period is based on the following findings. First
and foremost is the fact that if F-region polarization effects were
present, the relative motion of the plasma in the fingers and depleted
regions should have had an opposite sense from that observed. That is,
relative plasma motion should have been in a direction to reduce the
size of the fingers. Second, the spatial patterns of the slip velocity
vector and plasma density were not anticorrelated with each other, as
expected from polarization effects. Third, E-region Pedersen
conductance was high and the ratio of Pedersen conductance associated
with the blob to that with the background ionosphere was small. And
fourth, we found no obvious evidence of velocity shear. Velocity shear
is expected when the background Pedersen conductance is finite but small
compared to the blob Pedersen conductance [e.g., Zalesak et al., 1982].

Several researchers [e.g., Haerendel et al., 1967, 1969; Volk and
Haerendel, 1971; Shiau and Simon,1974; Vickrey and Kelley, 1982] have
shown that the gradient-drift instability (F-region polarization
electric fields) can be stabilized (short circuited) by the presence of

39

a conducting background. In this case, the F-region polarization electric field is shorted out by field-aligned currents that close through the conducting background. Rishbeth [1971] has shown the effectiveness of a sunlit E layer in keeping the F-region dynamo from operating during the day. Tsunoda [1985] has shown experimentally that equatorial F-region irregularities, produced by a process (collisional Rayleigh-Taylor instability) identical to the gradient-drift instability are strongly controlled by E-region conductivity effects.

Perkins and Doles [1975], Zalesak et al. [1982], and Huba et al. [1983] have shown that velocity shear effects set up by the electric field component along the plasma-density gradient result in damping of the gradient-drift instability. Both the blob analyzed in this paper and that reported by Tsunoda and Vickrey [1984] occurred in the presence of an electric-field component in the direction of the mean plasma-density gradient. Interestingly, we find little or no evidence in Figure 7(b) of velocity shear. If velocity shear was present, theory would predict the occurrence of tilted fingers away from perpendicularity with the blob major axis. The absence of tilt also supports the conclusion that F-region polarization electric fields were not present.

A remaining question is, what is the source of the irregular electric fields? A possible interpretation is that the blob analyzed in this paper was situated (or produced) at a magnetospheric boundary of some kind. This possibility arose while analyzing Figures 4, 7, and 8, i.e., plasma density profiles, electron temperatures, and ion velocities. As described earlier, electron temperature and ion velocity were substantially higher on the poleward side than on the equatorward side of the blob. A possibility is that the blob structure is simply an ionospheric signature of a magnetospheric process. For example, it is conceivable that wave structure and instability occurs at the magnetospheric boundary, producing irregular electric fields that map into the auroral ionosphere. Such a possibility has been suggested by several researchers [e.g., Fejer and Kelley, 1980; Vickrey and Kelley, 1982; Saflekos et al., 1985].

40

Lui et al. [1982] reported large-scale (200-900 km) undulations along the equatorward boundary of the diffuse aurora. They interpreted these optical observations in terms of surface waves propagating along the inner edge of the plasma sheet. While their results support the notion that magnetospheric wave structure could be observed in the ionosphere, their observations were made under conditions completely different from ours. Their structure is seen only in the afternoon-evening sector during magnetic storm activity.

We hope to shed more light on this matter after we analyze the HILAT satellite data obtained over the EISCAT scan sector during this experiment. Instruments on HILAT should provide further information regarding (1) the E layer Pedersen conductance, (2) the presence of field-aligned currents, (3) the latitudinal variations of electric field and particle characteristics, and (4) the characteristics of km-scale irregularities responsible for radio-wave scintillations.

ACKNOWLEDGMENTS

41

REFERENCES

Aggson, T., and J. P. Heppner, Observations of large transient magnetospheric electric fields, J. Geophys. Res., 82, 5155, 1977.

Amayenc, P., and G. Vasseur, Neutral winds deduced from incoherent scatter observations and their theoretical interpretation, J. Atmos. Terr. Phys., 34, 351, 1972.

Banks, P. M., C. L. Rino, and V. B. Wickwar, Incoherent scatter radar observations of westward electric fields and plasma densities in the auroral ionosphere, 1., J. Geophys. Res., 79, 25, 1974.

Banks, P. M., R. W. Schunk, and W. J. Raitt, NO^+ and O^+ in the high latitude F region, Geophys. Res. Lett., 1, 239, 1974.

Bates, H. F., Computed bounds on the F-region zonal wind during joule heating, J. Atmos. Terr. Phys., 40, 1123, 1978.

Bates, H. F., and T. D. Roberts, The southward midnight surge in F-layer wind observed with the Chatanika incoherent scatter radar, J. Atmos. Terr. Phys., 39, 87, 1977a.

Bates, H. F., and T. D. Roberts, A technique for using incoherent scatter to estimate F-region zonal winds during joule heating, J. Atmos. Terr. Phys., 39, 1293, 1977b.

Brekke, A., J. R. Doupnik, and P. M. Banks, Incoherent scatter measurements of E region conductivities and currents in the auroral zone, J. Geophys. Res., 79, 3773, 1974.

Cauffman, D. P., and D. A. Gurnett, Satellite measurements of high latitude convection electric fields, Space Sci. Rev., 13, 369, 1972.

Coffey, H. E., Geomagnetic and solar data, J. Geophys. Res., 89, 5666, 1984.

de la Beaujardiere, O., and R. A. Heelis, Velocity spike at the poleward edge of the auroral zone, J. Geophys. Res., 89, 1627, 1984.

Evans, J. V., Observations of F region vertical velocities at Millstone Hill, 1, Evidence for drifts due to expansion, contraction and winds, Radio Sci., 6, 609, 1971.

Fedder, J. A., and P. M. Banks, Convection electric fields and polar thermospheric winds, J. Geophys. Res., 77, 2328, 1972.

Fejer, B. G., and M. C. Kelley, Ionospheric irregularities, Rev. Geophys. Space Phys., 18, 401, 1980.

Folkestad, K., T. Hagfors, and S. Westerlund, EISCAT: An updated description of technical characteristics and operational capabilities, Radio Sci., 18, 867, 1983.

Fremouw, E. J., C. L. Rino, J. F. Vickrey, D. A. Hardy, R. E. Huffman, F. J. Rich, C.-I. Meng, K. A. Potocki, T. A. Potemra, W. B. Hanson, R. A. Heelis, and L. A. Wittwer, The HILAT program, EOS, 64, 163, 1983.

Gurnett, D. A., Injun 5 observations of magnetospheric electric fields and plasma convection, in Earth's Magnetospheric Processes, B. M. McCormac, ed., D. Reidel Publ. Co., Dordrecht-Holland, pp. 233-245, 1972.

Gurnett, D. A., and S.-I. Akasofu, Electric and magnetic field observations during a substorm on February 24, 1970, J. Geophys. Res., 79, 3197, 1974.

Haerendel, G., R. Lust, and E. Rieger, Motion of artificial ion clouds in the upper atmosphere, Planet. Space Sci., 15, 1, 1967.

Haerendel, G., R. Lust, E. Rieger, and H. Volk, Highly irregular artificial plasma clouds in the auroral zone, in Atmospheric Emissions, B. M. McCormac and A. Omholt, eds., p. 293, Van Nostrand Reinhold, N. Y., 1969.

Haggstrom, I., J. Murdin, and D. Rees, Determination of the thermospheric neutral wind from incoherent scatter radar measurements, preprint, 1984.

43

Hays, P. B., J. W. Meriwether, and R. G. Roble, Nighttime thermospheric winds at high latitudes, J. Geophys. Res., 84, 1905, 1979.

Hedin, A. E., J. E. Salah, J. V. Evans, C. A. Reber, G. P. Newton, N. W. Spencer, D. C. Kayser, D. Alcayde, P. Bauer, L. Cogger, and J. P. McClure, A global thermospheric model based on mass spectrometer and incoherent scatter data. MSIS 1. N2 density and temperature, J. Geophys. Res., 82, 2139, 1977.

Heelis, R. A., and W. B. Hanson, High latitude ion convection in the nighttime F region, J. Geophy. Res., 85, 1995, 1980.

Heppner, J. P., Electric field variations during substorms: OGO-6 measurements, Planet. Space Sci., 20, 1475, 1972.

Heppner, J. P., Empirical models of high latitude electric fields, J. Geophys. Res., 82, 1115, 1977.

Huba, J. D., S. L. Ossakow, P. Satyanarayana, and P. N. Guzdar, Linear theory of the $\underline{E} \times \underline{B}$ instability with an inhomogeneous electric field, J. Geophys. Res., 88, 425, 1983.

Kelley, M. C., J. F. Vickrey, C. W. Carlson, and R. Torbert, On the origin and spatial extent of high-latitude F-region irregularities, J. Geophys. Res., 87, 4469, 1982.

Keskinen, M. J., and S. L. Ossakow, Nonlinear evolution of plasma enhancements in the auroral ionosphere: 1. Long wavelength irregularities, J. Geophys. Res., 87, 144, 1982.

Lassen, K., J. R. Sharber, and J. D. Winningham, The development of auroral and geomagnetic substorm activity after a southward turning of the interplanetary magnetic field following several hours of magnetic calm, J. Geophys. Res., 82, 5031, 1977.

Linson, L. M., and J. B. Workman, Formation of striations in ionospheric plasma clouds, J. Geophys. Res., 75, 3211, 1970.

Lui, A. T. Y., C.-I. Meng, and S. Ismail, Large amplitude undulations on the equatorward boundary of the diffuse aurora, J. Geophys. Res., 87, 2385, 1982.

44

Nagy, A. F., R. J. Cicerone, P. B. Hays, K. D. McWatters, J. W. Meriwether, A. E. Belon, and C. L. Rino, Simultaneous measurement of ion and neutral motions by radar and optical techniques, Radio Sci., 9, 315, 1974.

Ossakow, S. L., and P. K. Chaturvedi, Current convective instability in the diffuse aurora, Geophys. Res. Lett., 6, 322, 1979.

Perkins, F. W., and J. H. Doles III, Velocity shear and the $\underline{E} \times \underline{B}$ instability, J. Geophys. Res., 80, 211, 1975.

Potemra, T. A., L. J. Zanetti, P. F. Bythrow, A. T. Y. Lui, and T. Iijima, By-dependent convection patterns during northward interplanetary magnetic field, J. Geophys. Res., 89, 9753, 1984.

Rees, D., N. Lloyd, P. J. Charleton, M. Carlson, J. Murdin, and I. Haggstrom, Comparison of plasma flow and thermospheric circulation over Northern Scandinavia using EISCAT and a Fabry-Perot interferometer, preprint, 1984.

Rino, C. L., V. B. Wickwar, P. M. Banks, S.-I. Akasofu, and E. Rieger, Incoherent scatter radar observations of westward electric fields, 2, J. Geophys. Res., 79, 4669, 1974.

Rishbeth, H., Polarization fields produced by winds in the equatorial F region, Planet. Space Sci., 19, 357, 1971.

Robinson, R. M., R. R. Vondrak, and T. A. Potemra, Electrodynamic properties of the evening-sector ionosphere within the region 2 field-aligned current sheet, J. Geophys. Res., 87, 731, 1982.

Robinson, R. M., R. T. Tsunoda, J. F. Vickrey, and L. Guerin, Sources of F region ionization enhancements in the nighttime auroral zone, J. Geophys. Res., submitted 1984.

Roble, R. G., and M. H. Rees, Time-dependent studies of the aurora: Effects of particle precipitation on the dynamic morphology of ionospheric and atmospheric parameters, Planet. Space Sci., 25, 991, 1977.

Roble, R. G., R. E. Dickinson, and E. C. Ridley, Global circulation and temperature structure of thermosphere with high-latitude convection, J. Geophys. Res., 87, 1599, 1982.

Saflekos, N. A., W. J. Burke, and P. F. Fougere, Large amplitude electric field fluctuations near the Harang discontinuity, Radio Sci., accepted 1985.

Schunk, R. W., and P. M. Banks, Auroral N2 vibrational excitation and the electron density trough, Geophys. Res. Lett., 2, 239, 1975.

Schunk, R. W., P. M. Banks, and W. J. Raitt, Effects of electric fields and other processes upon the nighttime high-latitude F layer, J. Geophyts. Res., 81, 3271, 1976.

Senior, C., R. M. Robinson, and T. A. Potemra, Relationship between field-aligned currents, diffuse auroral precipitation and the westward electrojet in the early morning sector, J. Geophys. Res., 87, 10469, 1982.

Shiau, J., and A. Simon, Barium cloud growth and striation in a conducting background, J. Geophys. Res., 79, 1895, 1974.

Simon, A., Instability of a partially ionized plasma in crossed electric and magnetic fields, Phys. Fluids, 6, 382, 1963.

Spiro, R. W., P. H. Reiff, and L. J. Maher, Jr., Precipitating electron energy flux and auroral zone conductances -- an empirical model, J. Geophys. Res., 87, 8215, 1982.

St.-Maurice, J. P., and W. B. Hanson, Ion frictional heating at high latitudes and its possible use for an in situ determination of neutral thermospheric winds and temperatures, J. Geophys. Res., 87, 7580, 1982.

Tsunoda, R. T., Control of the seasonal and longitudinal occurrence of equatorial scintillations by the longitudinal gradient in integrated E-region Pedersen conductivity, J. Geophys. Res., 90, 447, 1985.

Tsunoda, R. T., and J. F. Vickrey, Evidence of east-west structure in large-scale F-region plasma enhancements in the auroral zone, J. Geophys. Res., accepted 1984.

Tsunoda, R. T., R. M. Robinson, and C. Senior, Two types of plasma-density enhancements in the auroral F layer, Radio Sci., accepted 1984.

Vickrey, J. F., and M. C. Kelley, The effects of a conducting E layer on classical F region cross-field plasma diffusion, J. Geophys. Res., 87, 4461, 1982.

Vickrey, J. F., C. L. Rino, and T. A. Potemra, Chatanika/TRIAD observations of unstable ionization enhancements in the auroral F region, Geophys. Res. Lett., 7, 789, 1980.

Vickrey, J. F., R. R. Vondrak, and S. J. Matthews, The diurnal and latitudinal variation of auroral zone ionospheric conductivity, J. Geophys. Res., 86, 65, 1981.

Volk, H. J., and G. Haerendel, Striations in ionospheric ion clouds, 1, J. Geophys. Res., 76, 4541, 1971.

Wallis, D. D., and E. E. Budzinski, Empirical models of height integrated conductivities, J. Geophys. Res., 86, 125, 1981.

Watkins, B. J., and P. G. Richards, A theoretical investigation of the role of neutral winds and particle precipitation in the formation of the auroral F-region ionosphere, J. Atmos. Terr. Phys., 41, 179, 1979.

Weber, E. J., R. T. Tsunoda, J. Buchau, R. E. Sheehan, D. J. Strickland, W. Whiting, and J. G. Moore, Coordinated measurements of auroral zone plasma enhancements, J. Geophys. Res., submitted 1984.

Wickwar, V. B., J. W. Meriwether, P. B. Hays, and A. F. Nagy, The meridional thermospheric neutral wind measured by radar and optical techniques in the auroral region, J. Geophys. Res., 89, 10987, 1984.

Zalesak, S. T., S. L. Ossakow, and P. K. Chaturvedi, Nonlinear
equatorial spread F: The effect of neutral winds and background
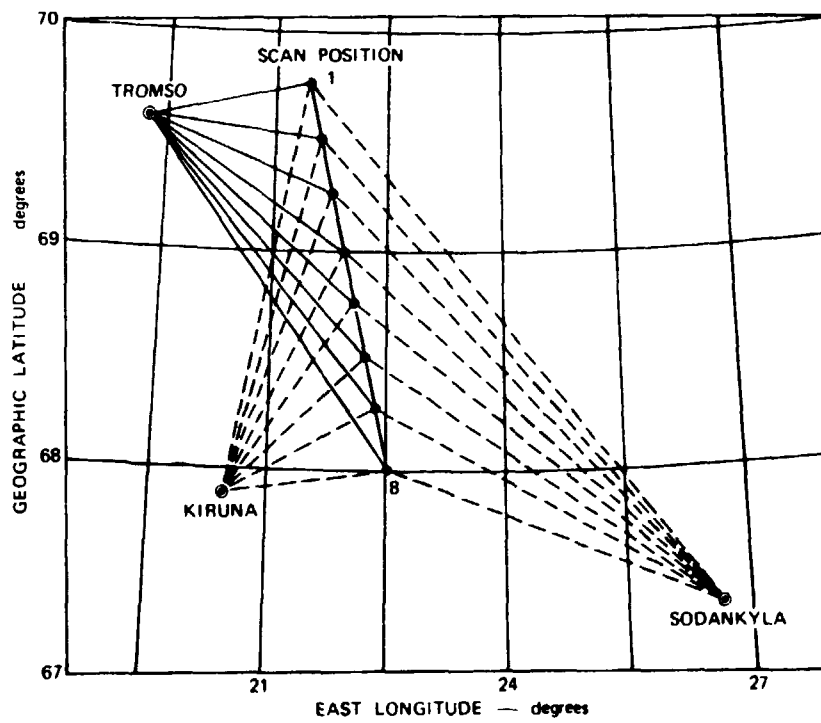Pedersen conductivity, J. Geophys. Res., 87, 151, 1982.

Figure 1. The EISCAT meridian-scan geometry showing the eight dwell positions at 300-km altitude.
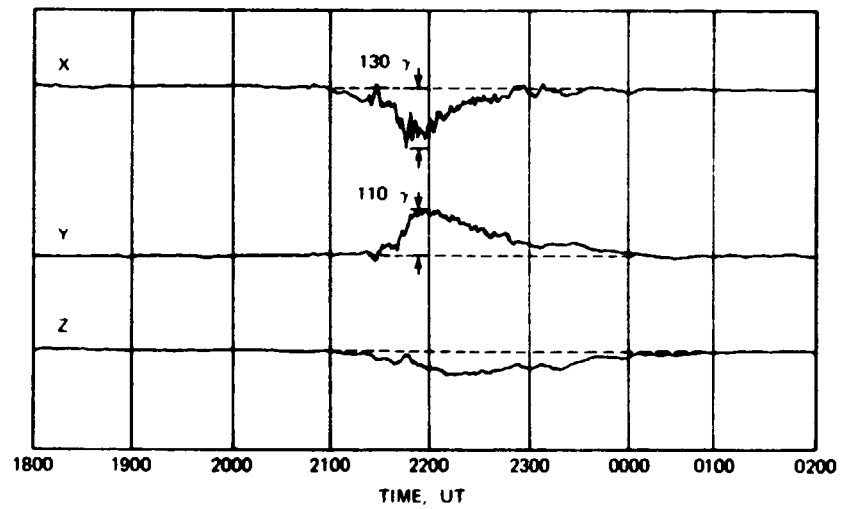
Figure 2. Kiruna magnetogram showing the isolated negative bay that occurred during the EISCAT experiment.
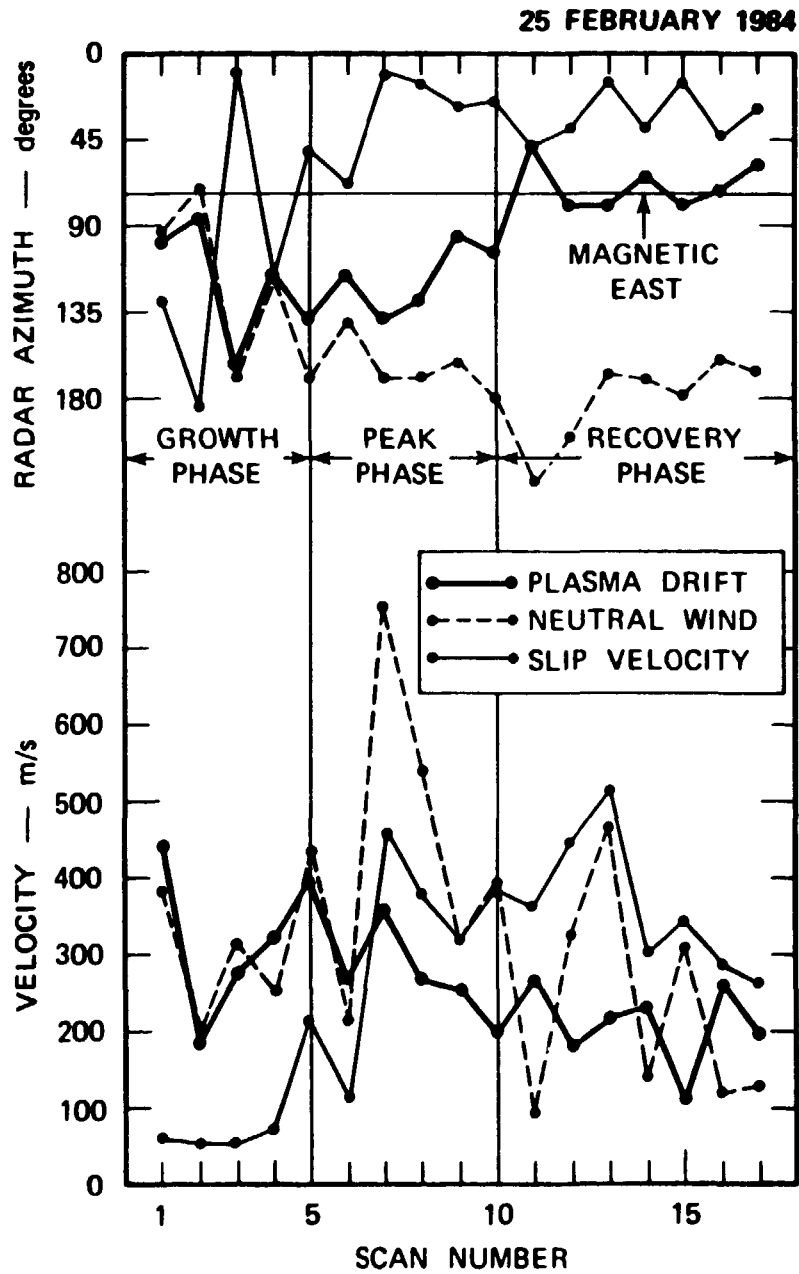
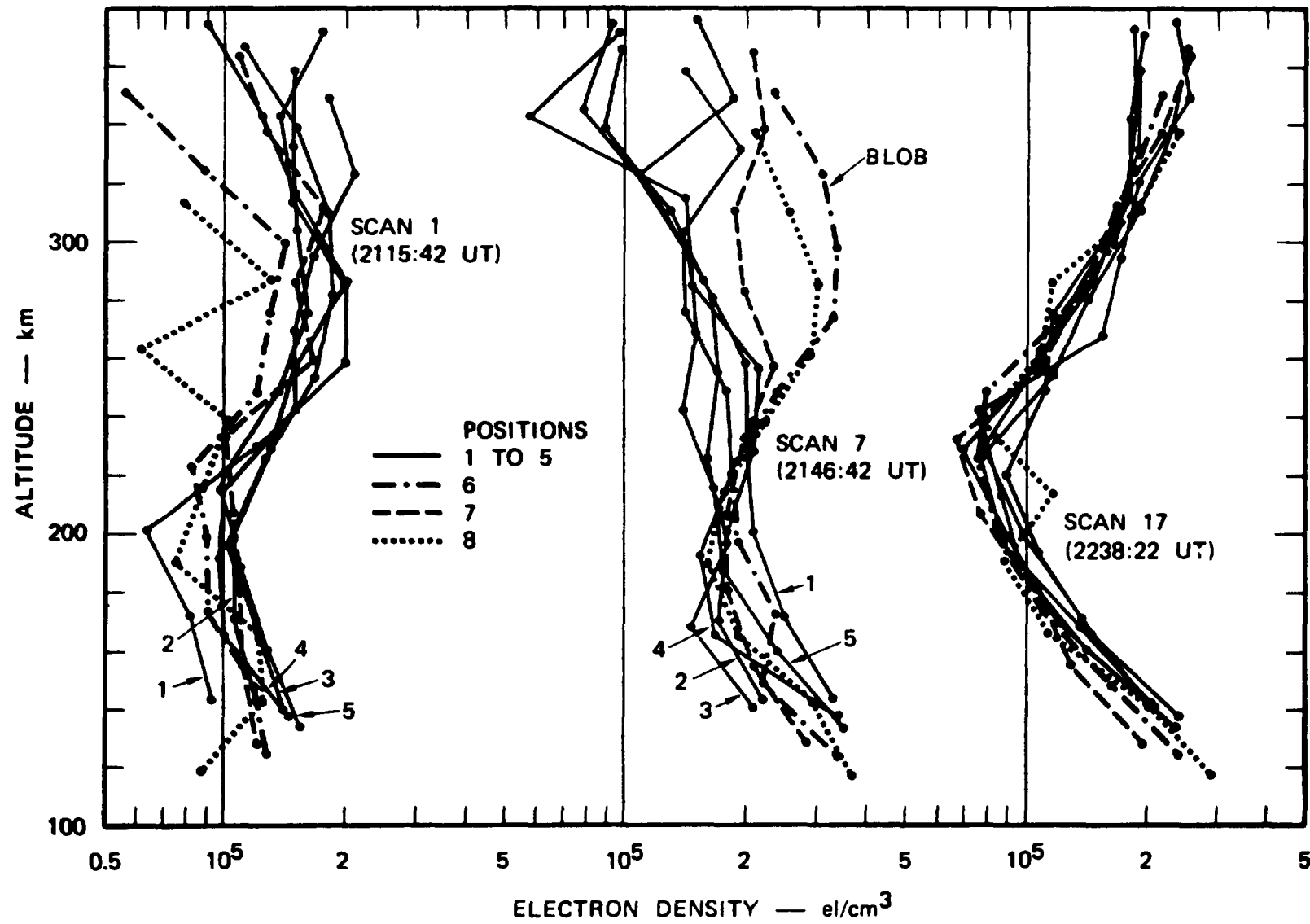Figure 3. Mean plasma drift, neutral wind, and slip velocity plotted as a function of substorm phase.

Figure 4. Plasma density profiles obtained during the growth phase (scan 1), the peak phase (scan 7), and the recovery phase (scan 17).
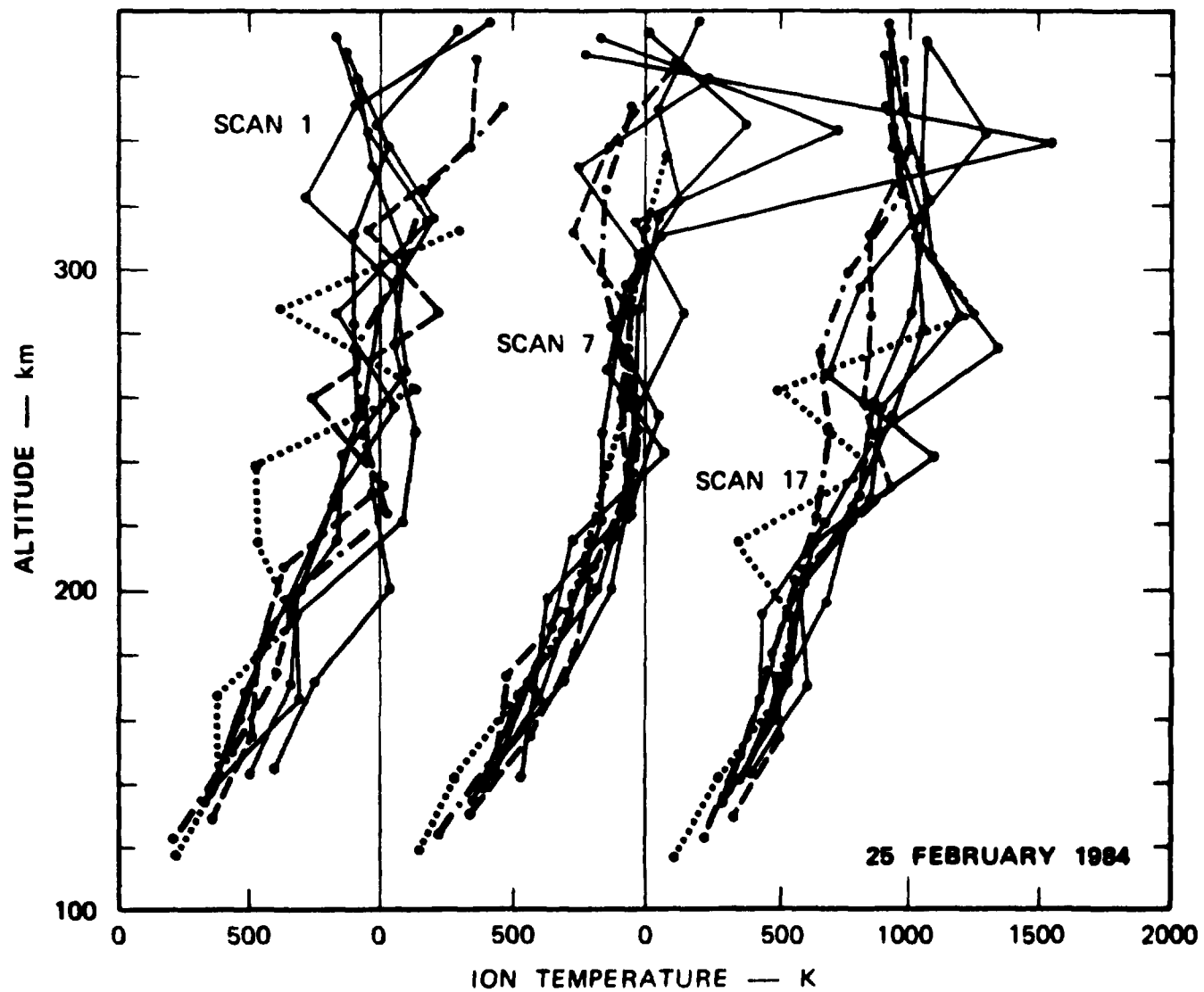
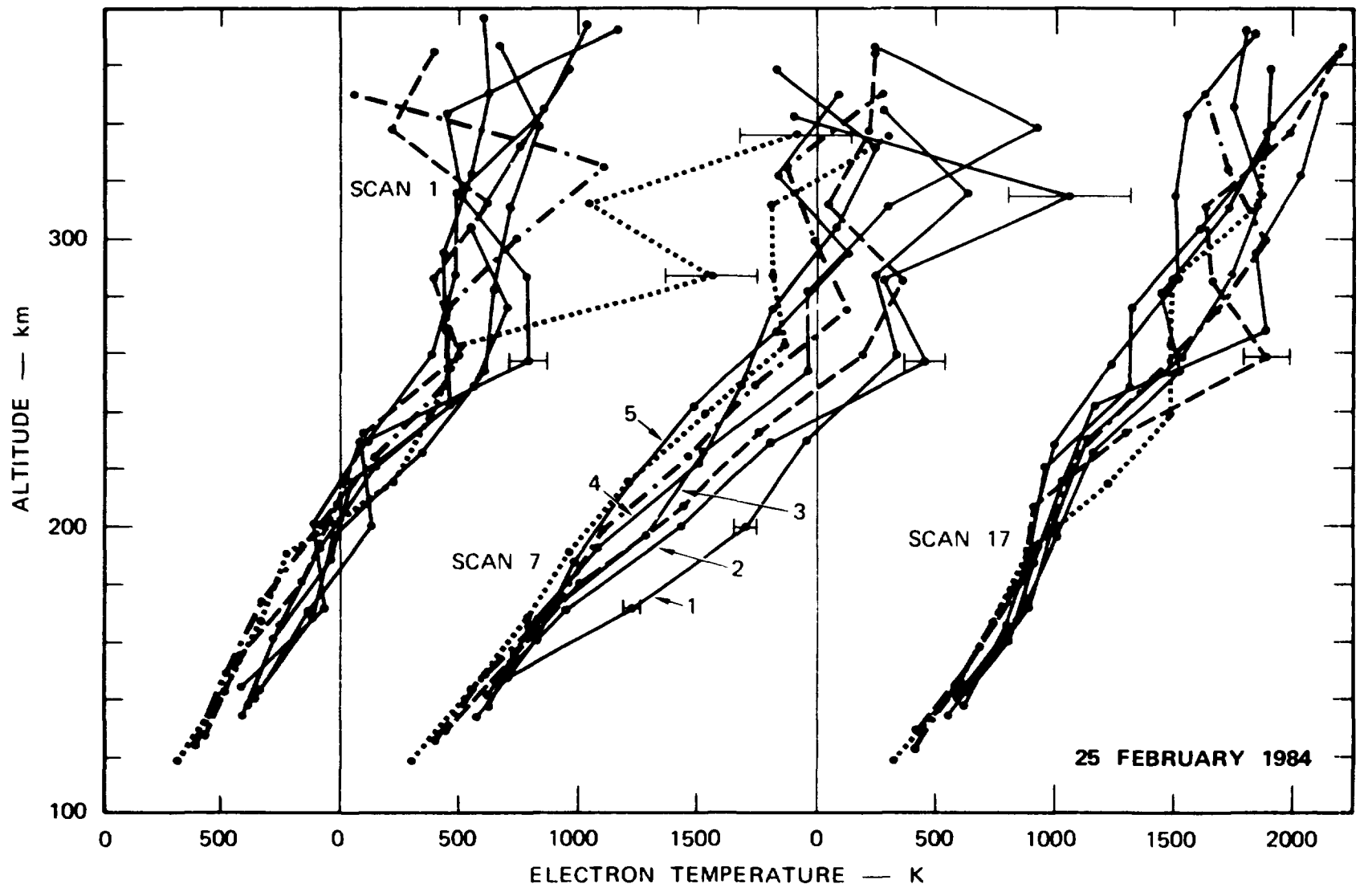Figure 5. Ion temperature profiles obtained during the three phases of the auroral substorm.

Figure 6. Electron temperature profiles obtained during the three phases of the auroral storm.
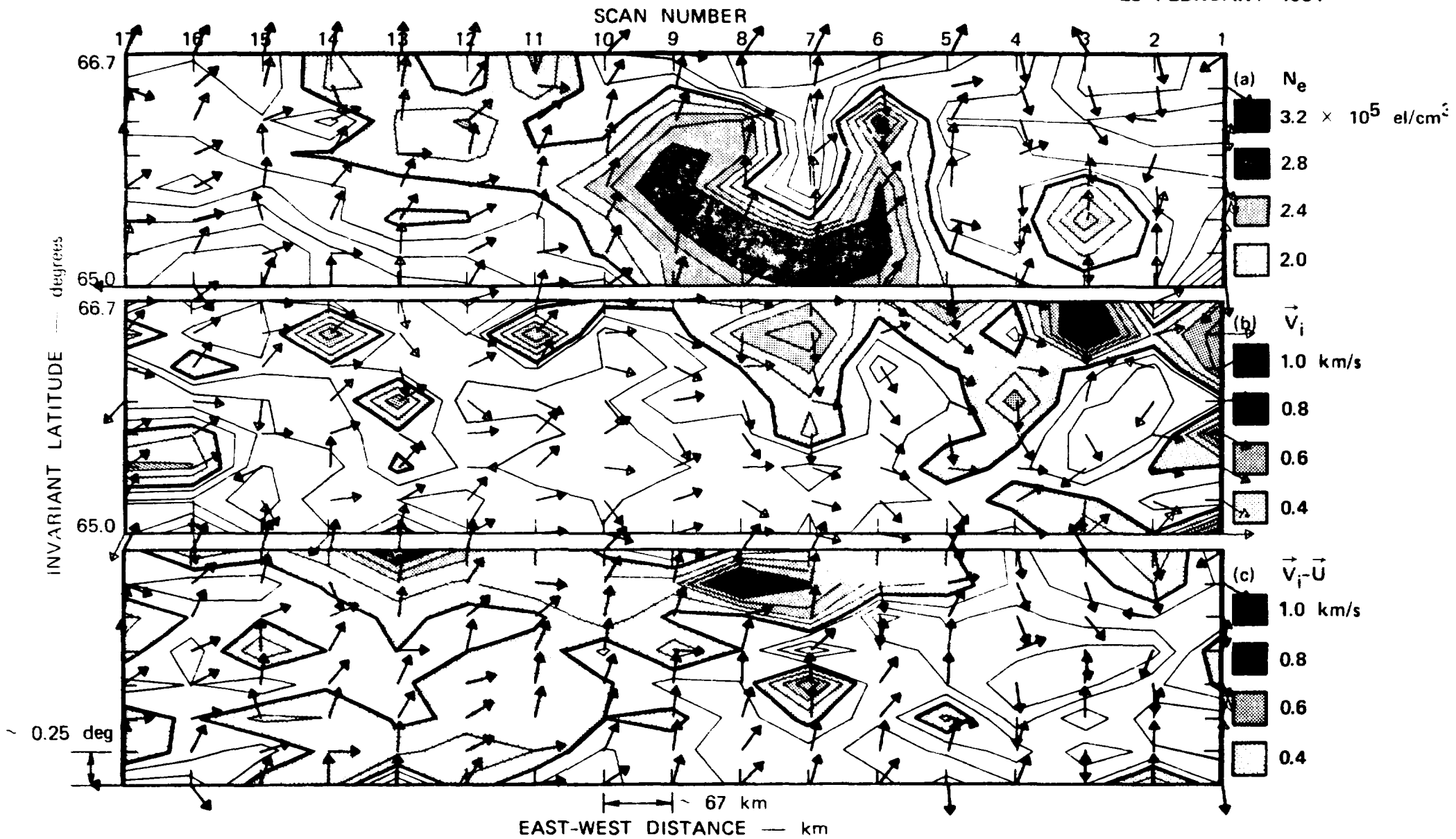
Figure 7. Two-dimensional patterns of plasma density, ion velocity, and slip velocity, in a plane transverse to the geomagnetic field at 300-km altitude.
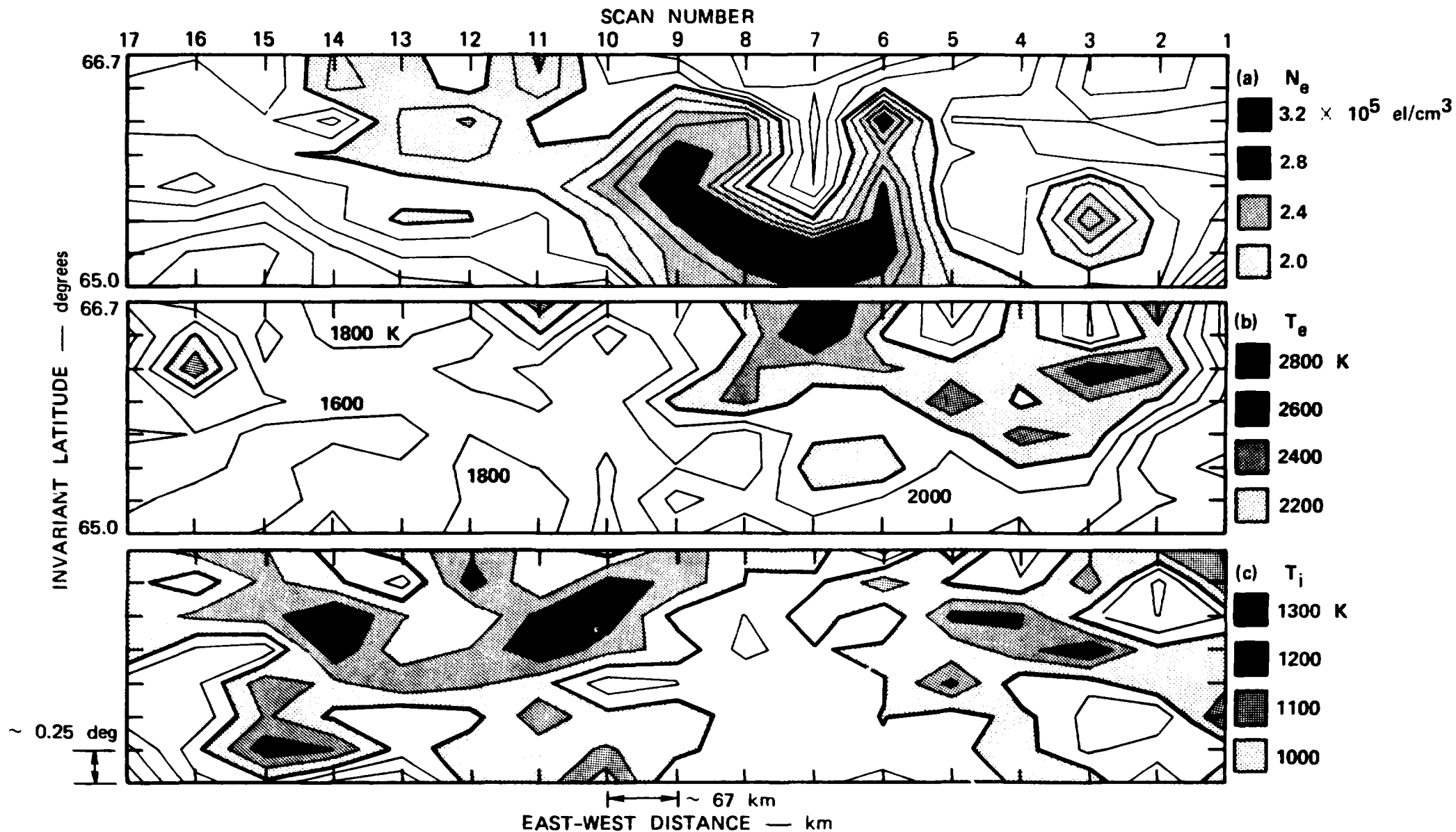
Figure 8. Two-dimensional patterns of plasma density, electron temperature, and ion temperature, in a plane transverse to the geomagnetic field at 300-km altitude.

Figure 9. Longitudinal variations in eastward plasma drift computed from line of sight velocity measurements at dwell position 1 from Tromso, during the 17 meridian scans.